Insights into the Formation and Evolution of Individual Compounds in the Particulate Phase during Aromatic Photo-Oxidation

Pereira, Kelly L.; Hamilton, Jacqueline F.; Rickard, Andrew R.; Bloss, William J.; Alam, Mohammed S.; Camredon, Marie; Ward, Martyn W.; Wyche, Kevin P.; Muñoz, Amalia; Vera, Teresa; Vázquez, Mónica; Borrás, Esther; Ródenas, Milagros

DOI:
10.1021/acs.est.5b03377

Document Version
Peer reviewed version

Citation for published version (Harvard):
Pereira, KL, Hamilton, JF, Rickard, AR, Bloss, WJ, Alam, MS, Camredon, M, Ward, MW, Wyche, KP, Muñoz, A, Vera, T, Vázquez, M, Borrás, E & Ródenas, M 2015, 'Insights into the Formation and Evolution of Individual Compounds in the Particulate Phase during Aromatic Photo-Oxidation', *Environmental Science & Technology*, vol. 49, no. 22, pp. 13168-13178. https://doi.org/10.1021/acs.est.5b03377

Article

Insights into the Formation and Evolution of Individual Compounds in the Particulate Phase during Aromatic Photo-oxidation

Kelly Louise Pereira, Jacqueline F Hamilton, Andrew Robert Rickard, William J. Bloss, Mohammed Salim Alam, Marie Camredon, Martyn W. Ward, Kevin P. Wyche, Amalia Munoz, Teresa Vera, Monica Vazquez, Esther Borras, and Milagros Ródenas

Environ. Sci. Technol., **Just Accepted Manuscript** • DOI: 10.1021/acs.est.5b03377 • Publication Date (Web): 16 Oct 2015

Insights into the Formation and Evolution of Individual Compounds in the Particulate Phase during Aromatic Photo-oxidation

Kelly L. Pereira[1], Jacqueline F. Hamilton[1], Andrew R. Rickard[1,2], William. J. Bloss[3], Mohammed S. Alam[3], Marie Camredon[4], Martyn W. Ward[1], Kevin. P. Wyche[5], Amalia Muñoz[6], Teresa Vera[6], Mónica Vázquez[6], Esther Borrás[6], Milagros Ródenas[6].*

[1]Wolfson Atmospheric Chemistry Laboratory, Department of Chemistry, University of York, York, UK. [2]National Centre for Atmospheric Science, University of York, UK. [3]School of Geography, Earth and Environmental Sciences, University of Birmingham, Birmingham, UK. [4]LISA, UMR CNRS/INSU 7583, University of Paris-Est Créteil and Paris Diderot, Créteil, France. [5]Air Environment Research, School Environment and Technology, University of Brighton, Brighton, UK. [6]CEAM-UMH, EUPHORE, Valencia, Spain.

[*]Corresponding author; e-mail: jacqui.hamilton@york.ac.uk. Phone: +44 (0)1904 324076. Fax: +44 (0) 1904 322516.

Abstract

Secondary organic aerosol (SOA) is well known to have adverse effects on air quality and human health. However, the dynamic mechanisms occurring during SOA formation and evolution are poorly understood. The time resolved SOA composition formed during the photo-oxidation of three aromatic compounds, methyl chavicol, toluene and 4-methyl catechol, were investigated at the European Photo-reactor. SOA was collected using a particle into liquid sampler and analysed offline using state-of-the-art mass spectrometry to produce temporal profiles of individual photo-oxidation products. In the photo-oxidation of methyl chavicol, 70 individual compounds were characterised and three distinctive temporal profile shapes were observed. The calculated mass fraction ($C_{i,aer}/C_{OA}$) of the individual SOA compounds showed either a linear trend (increasing/decreasing) or exponential decay with time. Substituted nitrophenols showed an exponential decay, with the nitro-group on the aromatic ring found to control the formation and loss of these species in the aerosol phase. Nitrophenols from both methyl chavicol and toluene photo-oxidation experiments showed a strong relationship with the NO_2/NO (ppbv/ppbv) ratio and were observed during initial SOA growth. The location of the nitrophenol aromatic substitutions was found to be critically important, with the nitrophenol in the photo-oxidation of 4-methyl catechol not partitioning into the aerosol phase until irradiation had stopped; highlighting the importance of studying SOA formation and evolution at a molecular level.

Introduction

Secondary organic aerosol (SOA) constitutes a significant proportion of ambient particulate matter[1-3] and exhibits substantial chemical complexity. The oxidation of a single volatile organic compound (VOC) forms a wide variety of multi-functional products of differing volatilities[4, 5]. These compounds may undergo numerous oxidation steps, forming a multitude

of oxidation products, only some of which may contribute to new particle formation and/or SOA growth. Furthermore, once a compound partitions into the condensed phase it can undergo further oxidation steps[6-9] and reactive transformations (non-oxidative processes, *i.e.* oligomerisation)[10-15], resulting in continually changing chemical composition and volatility[4]. The sheer number of VOCs present in the ambient atmosphere[16] and their continually evolving gas and particulate phase chemical composition, makes the identification of the species involved in SOA formation, growth and ageing, a complex and difficult task. Recent studies have found that extremely low volatility organic compounds (ELVOCs) can participate in new particle formation and drive nanoparticle growth[17-23]; a topic which has recently received considerable interest[2, 18, 24, 25]. Although, the detailed structural composition of these ELVOCs have not been identified[23, 26].

Atmospheric simulation chambers can afford mechanistic insight into SOA formation processes under simplified conditions. The oxidation of a single VOC precursor may be investigated in a controlled environment, providing significant insight into the mechanisms occurring during SOA formation and ageing. Bulk particle measurement techniques, such as aerosol mass spectrometry and derivatives[27], provide near-real time chemical speciation of non-refractory aerosol, allowing changes in particle oxidation to be observed[28, 29]. These techniques have been invaluable to our understanding of the chemical and physical transformations occurring during particle evolution. However, they cannot currently provide the detailed chemical composition and structural speciation that offline mass spectrometric techniques can offer[5, 30, 31].

Aromatic VOCs account for ~ 20 - 50 % of the non-methane hydrocarbon emissions in urban areas[32, 33], with toluene often observed to be the most abundant species[33-35]. Aromatic

hydrocarbons are considered to be one of the most important SOA precursors, contributing significantly to SOA formation[36-42]. Furthermore, their high reactivity makes them primary contributors to photo-chemical ozone formation[43, 44]. However, despite their important impact on urban air quality, aromatic photo-oxidation mechanisms are still poorly understood[45]. For aromatic compounds such as alkyl-benzenes, typically emitted from gasoline sources, new particle formation in chamber simulations has previously been shown to occur when the experiment moves from RO_2 + NO dominated regime to a RO_2 + HO_2 or RO_2 regime[46-49], suggesting that the species formed through this pathway are of sufficiently low volatility to initiate nucleation[4, 47]. This has previously been attributed to the formation of peroxides, although little compositional evidence has been found in aromatic systems to support this[23, 48]

SOA formation during the photo-oxidation of three mono-aromatic compounds, toluene (a predominantly anthropogenic VOC), 4-methyl catechol (anthropogenic oxygenated-VOC, OVOC) and methyl chavicol (biogenic OVOC, also known as estragole and 1-allyl-4-methoxybenzene) were investigated at the European Photoreactor in Valencia, Spain. Sub-micron aerosol samples were collected every 30 minutes using a particle into liquid sampler (PILS) and analysed offline using; high performance liquid chromatography ion-trap mass spectrometry (HPLC-ITMS), high performance liquid chromatography quadrupole time-of-flight mass spectrometry (HPLC-QTOFMS) and Fourier transform ion cyclotron resonance mass spectrometry (FTICR-MS). The use of a time resolved aerosol collection method followed by offline state-of-the-art mass spectrometric analysis, has allowed us to provide time resolved measurements with detailed chemical composition of the individual photo-oxidation products formed. From this, we are able to observe the partitioning, formation and loss of individual compounds in the particulate phase during SOA formation and ageing;

allowing us to observe the differences in the condensed phase evolution of individual species based on their structure and functionality.

Experimental

Chamber Simulation Experiments

Experiments were performed at the European Photoreactor (EUPHORE) in Valencia, Spain. Briefly, the EUPHORE facility consists of two ~ 200 m^3 hemispheric simulation chambers made of fluorinated ethylene propylene foil (FEP). Dry scrubbed air is used within the chamber and two large fans ensure homogenous mixing. Chamber temperature is near ambient and pressure is maintained at ~ 100 Pa above ambient. Further technical information can be found in the literature[45, 50-53]. Two sets of experiments were performed, during July 2009 as a part of the Toluene OXIdation in a Chamber (TOXIC) project and during May 2012 as a part of the Atmospheric Chemistry of Methyl Chavicol (ATMECH) project. VOC precursors investigated, initial VOC/NO_x mixing ratios and average chamber humidity and temperature for the experiments discussed, are shown in Table 1.

The chamber was cleaned before each experiment by flushing with dry scrubbed air. The VOC precursor was introduced into the chamber through a heated air stream. Photo-oxidation experiments were performed, where no additional source of $^{\bullet}OH$ radicals were added into the chamber, using wall chemistry to initiate photo-oxidation[54, 55]. A range of instruments were used to monitor chamber pressure (Barometer, model AIR-DB-VOC), humidity (Hygrometer Watz, model Walz-TS2), temperature (temperature sensor, model PT100), solar intensity ($j(NO_2)$ Filter radiometer), NO_x (Teledyne API, model NO_X_API-T200UP; photolytic converter) and O_3 (Monitor Labs, model 9810). During the TOXIC project, precursor degradation and product formation was monitored using a Fourier transform infra red

spectrometer (FTIR, Nicolet Magna, model 550) coupled to a white-type mirror system (optical path length 616 m) and a chemical ionisation reaction time-of-flight mass spectrometer (CIR-TOF-MS, Kore Technology). In the ATMECH project, the CIR-TOF-MS was replaced with proton transfer reaction mass spectrometry (PTR-MS, Ionikon Analytik). SOA mass, size and number concentrations were measured using a scanning mobility particle sizer (TSI Incorporated, model 3080) consisting of a differential mobility analyzer (model 3081) and a condensation particle counter (model 3775).

Aerosol Sampling and Analysis

The analytical procedures are discussed in more detail in Pereira et al. (2014)[56] with a brief summary given here. Aerosol samples were collected every 30 minutes using a PILS (Brechtel Manufacturing, model 4002). The PILS inlet was connected to the chamber outlet using 1.5 metres of 1/3" stainless steel tubing. PM_1 aerosol samples were collected using an impactor at an average flow rate of 12 L min^{-1}. The PILS sample and wash flow was set to 200 μL min^{-1} and 240 μL min^{-1}, respectively, and consisted of optima LC-MS grade water (Fisher Scientific, UK). After sample collection, PILS vials were securely sealed, wrapped in foil to minimise potential degradation from photolysis and stored at – 20 °C until analysis. Prior to analysis, PILS samples were evaporated to dryness using a V10 vacuum solvent evaporator (Biotage, USA) and re-suspended in 50:50 methanol:water (optima LC-MS grade, Fisher Scientific, UK).

SOA composition was investigated using an Agilent 1100 series HPLC (Berkshire, UK) coupled to a HTC Plus ion trap mass spectrometer (IT-MS, Bruker Daltonics, Bremen, Germany). A reversed phase Pinnacle C_{18} 150 mm x 4.6 mm, 5 μm particle size column (Thames Resteck, UK) was used. The mobile phase consisted of water (optima LC-MS

125 grade) with 0.1 % formic acid (Sigma Aldrich, UK) and methanol (optima LC-MS grade,
126 Fisher Scientific UK). The MS was operated in alternating polarity mode, scanning from *m/z*
127 50 to 600. Tandem MS (collision induced dissociation, CID) was achieved through the
128 automated MS^2 function within the Esquire software (Bruker Daltonics, software version
129 5.2). In addition to the HPLC-ITMS, the ATMECH PILS samples were further investigated
130 using a solariX FTICR-MS with a 9.4-T superconducting magnet (Bruker Daltonics,
131 Coventry, UK) and a Dionex ultimate 3000 HPLC (Thermo Scientific Inc, UK) coupled to an
132 ultra high resolution QTOFMS (maXis 3G, Bruker Daltonics, Coventry, UK). The HPLC-
133 QTOFMS used the same reversed phase column and mobile phase composition as described
134 above for the HPLC-ITMS analysis. Spectral analysis was performed using DataAnalysis 4.0
135 software (Bruker Daltonics, Breman, Germany).
136
137 **Results and Discussion**
138 Initially, the PILS samples were screened for SOA species using HPLC-ITMS. Any
139 compounds present before the introduction of the VOC precursor and NO into the chamber
140 were excluded from further analysis. Only compounds that displayed changes in their
141 chromatographic peak areas were investigated further. Peak areas of the observed SOA
142 compounds were measured in each 30 minute PILS sample, allowing the temporal evolution
143 of individual species in the particulate phase to be observed. The temporal profiles of the
144 VOC precursor, NO, NO_2, O_3 and the SOA mass formed, during the experiments can be
145 found in the SI, Figure S1. The observed first generation gas-phase photo-oxidation products
146 are shown in the SI, Figure S2.
147
148 **Photo-oxidation of Methyl Chavicol**

Initially, the SOA composition formed during the photo-oxidation of methyl chavicol, experiment $MC_{[high]}$ (Table 1) was investigated. In this experiment, 460 ppbv of methyl chavicol and 92 ppbv of NO were added into the chamber and the chamber exposed to sunlight. The maximum SOA mass formed was 283 μg m^{-3}, resulting in an SOA yield of 31 %[56] (corrected for chamber wall loss and dilution). In total, 79 SOA compounds were observed in the PILS SOA samples using HPLC-ITMS; including 20 SOA compounds in addition to those previously reported[56]. Temporal profiles were created for 70 of the 79 SOA species. The other 9 compounds were excluded owing to the majority of chromatographic peaks observed being below the limit of detection (defined as S/N = 3). The temporal profiles of the individual SOA species varied considerably, with different rates of aerosol partitioning, formation and loss observed. Nevertheless, three main temporal profile shapes could be distinguished.

The majority of SOA compounds displayed a relatively slow increase in their particle phase concentration, following initial aerosol growth, after which their concentration either plateaued or began to decrease towards the end of the experiment (~ 4 hours). Of the 79 SOA compounds observed, 47 species displayed this type of temporal profile (hereafter referred to as TP1) and an example is shown in Figure 1A. The majority of these compounds were first observed in the aerosol phase between 71 to 101 minutes into the experiment, when the SOA mass in the chamber was rapidly increasing (63 to 188 μg m^{-3}, Figure 1G). All of these compounds displayed a gradual increase in their particulate phase concentration, with the majority reaching maximum concentration at ~ 175 minutes into the experiment, when SOA formation in the chamber had plateaued. The compound structures of 5 of these species have been determined[56] and were identified as; (3-hydroxy-4-methoxyphenyl)acetic acid, 3-(3-hydroxy-4-methoxyphenyl)propane-1,2-diol, 4-methoxybenzoic acid, 3-hydroxy-4-

methoxybenzoic acid and 2-hydroxy-3-(3-hydroxy-4-methoxyphenyl)propanal. The saturation concentrations (C^* (μg m^{-3}))[57] of these compounds were calculated (see SI) and determined to range from 1.23 to 917 μg m^{-3}, characterising these species as intermediate- to semi-VOCs (IVOC-SVOC). The compound structures, their most likely mechanistic generation and the time period these compounds were first observed in the aerosol phase are shown in SI, Table S1.

The mass fraction (y_i) of a species in the aerosol phase can be calculated by dividing the measured concentration of species (i) in the condensed phase ($C_{i,aer}$ (μg m^{-3})) by the average SOA mass formed (C_{OA} (μg m^{-3})) in each PILS sampling time period ($y_i = C_{i,aer}/C_{OA}$)[58]. The measured mass fraction (y_i) of 4-methoxybenzoic acid (typical TP1 species) in the condensed phase displayed a linear increase (R^2 = 0.9938) with time, after ~101 minutes into the experiment (SOA mass > 191 μg m^{-3}), as shown in Figure 1B. The gas-phase concentration of 4-methoxybenzoic acid could not be determined due to the extensive fragmentation of this species in the PTR-MS. However based on the absorptive partitioning theory[58], a positive linear relationship between y_i and time would only be observed if the gas-phase concentration ($C_{i,gas}$ (μg m^{-3})) of this species continued to increase linearly throughout the experiment; where $C_{i,gas} = (C_i^* \times C_{i,aer})/C_{OA}$[58]. It is therefore suggested that the positive linear relationship observed here, is a result of a faster gas-phase formation rate than loss, resulting in progressive absorptive partitioning into the aerosol phase as $C_{i,gas}$ and C_{OA} increases[4, 59, 60]. The majority of the TP1 compounds displayed a linear relationship with the SOA mass, suggesting the partitioning of these species into the aerosol phase were also driven by absorptive partitioning, which considering the relatively high volatility of the identified species, would appear to be a reasonable explanation. There were however, variations in the timing, duration and rate of increasing/decreasing y_i, most likely owing to the different rates

of formation and loss of these compounds in the gas-phase and their volatility. Reactive uptake *via* in-particle formation processes[58] is also a possibility, however it is unclear if the formation of the TP1 species (*i.e.* 59 % of observed compounds) through in-particle phase reactions would result in a linear relationship with the SOA mass.

The second type of temporal profile shape observed (TP2) displayed a rapid increase and then decrease in aerosol phase concentration, as shown in Figure 1C. These species were short lived, remaining in the aerosol phase for a maximum of 2.5 hours, and could not be detected in the aerosol samples taken at the end of the experiment. Only 3 compounds displayed this type of temporal profile and the structure of one was identified as (4-methoxyphenyl)acetic acid[56]. The two unidentified species consisted of one highly oxygenated compound, $C_8H_{12}O_8$ (O:C = 1) and one species, $C_{11}H_{14}O_4$, which contained one more carbon atom than the original VOC precursor. All of these compounds reached peak concentration up to 30 minutes after partitioning into the aerosol phase (*i.e.* in the following PILS sample) and displayed a rapid loss process after maximum concentration was observed. The rapid decrease in the aerosol phase concentration observed for these compounds could be due to a variety of loss processes, such as; (i) photolysis or further reaction of the compound in the gas-phase resulting in re-volatilisation from the particle phase; and/or, (ii) in-particle phase/heterogeneous reactions.

For the identified species, (4-methoxyphenyl)acetic acid, photolytic degradation is considered to be negligible[61]. However, the identification of an oxidation product, with an additional $^{\bullet}$OH group on the aromatic ring (3-hydroxy-4-methoxyphenyl)acetic acid[56] indicates further that gas-phase and/or heterogeneous reactions are occurring. The measured mass fraction (y_i) of (4-methoxyphenyl)acetic acid in the condensed phase decreased linearly

224 with time (R^2 = 0.9903, Figure 1D). Assuming equilibrium partitioning, the temporal
225 evolution of (4-methoxyphenyl)acetic acid in the aerosol phase can be predicted by using
226 $C_{i\text{aer}} = (C_{OA} \times C_{i\text{gas}})/C^{*58}$. The predicted and measured particulate phase temporal profiles of
227 (4-methoxyphenyl)acetic acid are shown in the SI, Figure S3. There are clear differences
228 between the two profiles, with the predicted temporal profile timing and shape more closely
229 resembling TP1 than a TP2 evolution. This suggests that for these species an additional loss
230 process is occurring, such as in-particle phase/heterogeneous reactions, leading to a deviation
231 from gas-particle equilibrium partitioning.
232
233 The third type of temporal profile shape (TP3) was similar to TP2 discussed above, except
234 these compounds appeared in the aerosol phase earlier in the experiment (between 41 to 71
235 minutes) and a different rate of decreasing aerosol concentration was observed (Figure 1E).
236 Interestingly, all 8 species that displayed this type of temporal profile contained nitrogen.
237 Seven of these organic nitrogen (ON) species were first observed in the aerosol phase when
238 initial SOA growth was observed in the chamber (41 - 71 minutes into the experiment, Figure
239 1E) and reached peak concentration within the next 30 minutes. The complex re-
240 arrangements observed for these compounds during CID in the mass spectrometer made the
241 structural identification particularly difficult. However, one of these compounds was
242 identified as 3-(5-hydroxy-4-methoxy-2-nitrophenyl)propane-1,2-diol[56] and the structures of
243 two others have been tentatively assigned as substituted nitrophenols; 5-methoxy-4-nitro-2-
244 (prop-2-en-1-yl)phenol and 1-hydroxy-3-(2-hydroxy-4-methoxy-5-nitrophenyl)propan-2-one
245 (see the SI for the discussion of the structural assignment). The compound structures, time
246 period these compounds were first observed in the aerosol phase and their proposed
247 mechanistic generations are shown in SI Table S2. The calculated saturation concentrations
248 and O:C ratios of the structurally identified compounds ranged from 4.37×10^2 to 2.86×10^{-3}

249 μg m^{-3} and 0.4 to 0.6 respectively, classifying these species as semi- to low volatility organic
250 compounds (SVOC-LVOC)[39].
251
252 The decrease in the particulate phase concentration observed for these species may be the
253 result of a number of competing processes, such as; the low formation rates of the gas-phase
254 nitro-aromatics as the NO_2 concentration is depleted in the chamber (as NO_x is not
255 replenished), photolysis/further reaction of the gas-phase species which may lead to re-
256 volatilisation from the aerosol phase and/or in-particle phase/heterogeneous chemistry.
257 However, the observation of only one additional nitrogen containing compound later in the
258 experiment suggests that either; (i) these compounds are entirely removed from the aerosol
259 phase through re-volatilisation and do not partition back into the aerosol phase, or; (ii) upon
260 further reaction lose nitrogen. The complete removal of these species from the particulate
261 phase through re-volatilisation would appear unlikely due to the low volatility of these
262 compounds. A more likely explanation for the lack of additional nitrogen containing
263 oxidation products, is that upon further reaction, nitrogen is being lost. A number of recent
264 studies have found that nitrophenols can lose HONO in the gas phase[62-64];, potentially a
265 similar loss mechanism could also occur in the condensed phase, explaining why only one
266 additional nitrogen containing oxidation product was observed. In contrast to the temporal
267 profiles discussed above, the measured mass fraction (y_i) of all of the TP3 compounds
268 displayed a decreasing exponential relationship with time ($R^2 > 0.9432$). This relationship
269 can be observed in Figure 1F for the identified species, 3-(5-hydroxy-4-methoxy-2-
270 nitrophenyl)propane-1,2-diol. The reason why an exponential relationship is observed is
271 currently unclear but possible influences are discussed further below.
272
273 **Evolution of Nitrophenols**

SOA was first observed in the PILS sample collected between 41 to 71 minutes into the experiment (SI Figure S4). In this sample, 13 SOA compounds were observed and included eight ON species ($C_9H_{11}NO_9$ (t_R = 11.8), $C_9H_{11}NO_9$ (t_R = 12.8), $C_{10}H_9NO_3$, $C_{10}H_{13}NO_6$, $C_{10}H_{11}NO_6$, $C_{10}H_{11}NO_4$, $C_5H_7NO_6$ and $C_{10}H_{17}NO_3$), one oligomer ($C_{18}H_{20}O_{12}$), three oxidised compounds ($C_{10}H_{14}O_3$, $C_{11}H_{18}O_5$ and $C_{10}H_{12}O_5$), and one compound at molecular weight (MW) 120 g mol^{-1}; whose molecular formula could not be assigned using only the elements C, H, N and O. Of the ON compounds, the structures of three were identified as substituted nitrophenols (3-(5-hydroxy-4-methoxy-2-nitrophenyl)propane-1,2-diol[56], (SI Table S2, compound 1), 1-hydroxy-3-(2-hydroxy-4-methoxy-5-nitrophenyl)propan-2-one (SI Table S2, compound 2) and 5-methoxy-4-nitro-2-(prop-2-en-1-yl)phenol (SI Table S2, compound 3), see SI for the structural assignment) and a further three displayed characteristic fragmentation patterns suggesting these compounds contained a resonance stabilised ring structure and a nitro group ($C_9H_{11}NO_9$ (t_R = 11.8), $C_9H_{11}NO_9$ (t_R = 12.8) and $C_{10}H_9NO_3$), indicating that these species were also likely to be substituted nitrophenols.

The particulate phase temporal profiles of the nitrophenols (both identified and suspected) and the NO_2/NO (ppbv/ppbv) ratio were found to be remarkably similar, as shown for example in Figure 2. All of the structurally identified nitrophenols were observed to have different degrees of oxidation on the hydrocarbon chain substituent, with a diol, hydroxy-carbonyl and unreacted alkene (same functionality as the starting precursor, methyl chavicol) observed. Nevertheless, all of these compounds displayed the same temporal profile shape and relationship with the NO_2/NO ratio, suggesting that it is the NO_2 group on the aromatic ring that controls the partitioning, formation and loss of these species in the particulate phase. This can be further supported by considering the two remaining ON compounds observed, $C_5H_7NO_6$ and $C_{10}H_{17}NO_3$. Both of these compounds displayed a TP1 temporal profile shape

299 rather than the nitrophenol TP3 shape. Based on the molecular formulae, these species cannot
300 contain a resonance stabilised ring structure (*i.e.* they are ring opened species) with $C_5H_7NO_6$
301 containing too few carbon atoms, and $C_{10}H_{17}NO_3$ containing too many hydrogen atoms.
302 Thus, these compounds cannot be substituted nitrophenols, potentially explaining why a TP3
303 evolution and relationship with the NO_2/NO ratio was not observed for these species.
304
305 The structurally identified nitrophenols were characterised as SVOCs to LVOCs, with 3-(5-
306 hydroxy-4-methoxy-2-nitrophenyl)propane-1,2-diol just fractionally outside the nucleator
307 (ELVOC) region proposed in Donahue et al. (2013)[26]. Converting the calculated saturation
308 concentrations of 3-(5-hydroxy-4-methoxy-2-nitrophenyl)propane-1,2-diol ($C^* = 2.86 \times 10^{-3}$
309 $\mu g\ m^{-3}$) and 1-hydroxy-3-(2-hydroxy-4-methoxy-5-nitrophenyl)propan-2-one (1.09×10^{-1} μg
310 m^{-3}) into gas-phase mixing ratios, concentrations of 0.29 pptv and 11.05 pptv, respectively,
311 would be required for these compounds to reach their saturation concentrations and partition
312 into the aerosol phase without any absorptive mass present. Considering the initial mixing
313 ratio of methyl chavicol (460 ppbv), the saturation concentrations of these suspected third
314 generation products would appear to be easily obtainable. Furthermore, the molecular
315 formulae of two of the suspected nitrophenols were found to have one less carbon atom than
316 these species, but considerably more oxygen atoms (O_9 instead of O_6 ($C_9H_{11}NO_9$, O:C =1))
317 indicating these compounds are also likely to be of similar or lower volatility. The low
318 saturation concentrations of these compounds coupled with the observation of these species
319 in the aerosol phase during initial SOA growth, as shown in Figure 3, suggests these species
320 could potentially be involved new particle formation and/or SOA growth.
321
322 **Toluene and 4-Methyl Catechol: Nitrophenol Evolution**

Owing to the clear importance of nitrophenols in methyl chavicol SOA formation, two other aromatic systems, toluene and 4-methylcatechol were also investigated. Two toluene photo-oxidation experiments were investigated; (i) Tol_{low}, a VOC/NO_x ratio of ~ 13, where 535 ppbv of toluene and 41 ppbv of NO was added into the chamber, and; (ii) Tol_{mod}, a higher VOC/NO_x ratio of ~ 5, where 560 ppbv of toluene and 105 ppbv of NO was added into the chamber (Table 1). The maximum amount of SOA mass formed was 22.3 μg m^{-3} in Tol_{low} and 32.8 μg m^{-3} in Tol_{mod}, with SOA yields of 3.4 % and 5.4 % respectively (corrected for wall loss and chamber dilution). In both experiments, two nitrogen containing compounds were observed in the PILS SOA samples and are assigned as 2-methyl-4-nitrophenol ($C_7H_7NO_3$, MW 153 g mol^{-1}), a second generation product, and methyl nitro-catechol ($C_7H_7NO_4$, MW 169 g mol^{-1}), a third generation product. Both of these compounds are known toluene photo-oxidation products[65-69]. The identification of 2-methyl-4-nitrophenol was confirmed from the chromatographic retention time and fragmentation patterns of the commercially available standard. The exact locations of the aromatic substitutions of methyl nitro-catechol are unclear and are discussed in the SI, but based on known gas-phase mechanisms and the structural elucidation of the mass spectral fragmentation patterns, the most likely structure is 3-methyl-4-nitrocatechol.

The temporal profiles of 2-methyl-4-nitrophenol and methyl nitro-catechol were observed to follow the same TP3 shape observed previously for the methyl chavicol nitrophenols. Again, both of these compounds displayed a relationship with the temporal profile of the NO_2/NO ratio (SI Figure S5 and S6). The saturation concentrations of 2-methyl-4-nitrophenol and methyl nitro-catechol (calculation based on 3-methyl-4-nitrocatechol) were determined as 1.12×10^5 and 1.41×10^3 μg m^{-3}, respectively, characterising these species as IVOCs. The gas-phase concentrations of 2-methyl-4-nitrophenol and methyl nitro-catechol in both toluene

348 experiments are not known. However, in order for 2-methyl-4-nitrophenol and methyl nitro-
349 catechol to partition into the aerosol phase without any absorptive mass present, gas-phase
350 concentrations of 17.95 ppmv and 0.20 ppmv, respectively, would be required (based on their
351 calculated saturation concentrations); well in excess of the amount of toluene reacted prior to
352 SOA formation in both experiments. Providing some absorptive mass is present, a gaseous
353 species can partition some of its mass into the aerosol phase below its saturation
354 concentration[4, 59, 60]. However, even taking this into account, equilibrium partitioning cannot
355 describe the observation of these relatively volatile species in the aerosol phase during initial
356 aerosol formation and growth (see SI for the supporting calculations and SI Figures S7 and
357 S8).
358
359 The reason why these IVOCs are observed in the aerosol phase during initial aerosol
360 growth is currently unclear. However, a recent study has also observed a similar phenomenon
361 with nitrophenols formed from the photo-oxidation of benzene[70]. Using high resolution time-
362 of-flight aerosol mass spectrometry (HR-TOF-AMS), Sato et al. (2012) measured
363 nitrophenols from the onset of SOA nucleation and observed them to rapidly decrease in
364 concentration over the first hour[70]. The composition of these compounds was determined
365 from the collection of SOA onto filter samples, followed by offline HPLC-TOFMS
366 analysis[70]. Whilst no reference to volatility was made in their study, the two nitrophenols
367 identified (4-nitrophenol and 4-nitrocatechol) are of even higher volatility (calculated C^* =
368 3.19×10^5 and 4.70×10^3 $\mu g\ m^{-3}$) than the species identified in this study, owing to the lack of
369 a methyl group on the aromatic ring. Furthermore, Sato et al. (2012) observed that from the
370 onset of SOA nucleation to the first 60 minutes of their experiment, nitrophenol formation
371 was almost independent of the amount of absorptive mass present[70], which is in agreement

372 with the results shown here. One possible explanation for these observations is the formation
373 of gas-phase clusters.
374
375 A number of studies have shown phenol-phenol or phenol-water clusters can form in the
376 gas-phase and produce stable clusters through hydrogen bonding[71-74]. Theoretical simulations
377 predict the stability of phenol-water clusters to be comparable to that of water clusters,
378 exhibiting similar hydrogen bonding energies[72, 74]. Whilst no studies have investigated
379 nitrophenol gas-phase clustering, these compounds are known to form both intra- and inter-
380 molecular hydrogen bonds; with very strong intra-molecular hydrogen bonding observed
381 between the nitro and hydroxyl group (C-NO—HO-C)[75-77]. Such interactions could result in
382 stabilised cluster formation and new particle formation, potentially accounting for the
383 observations shown in Sato et al. (2012)[70] and in this study; although this remains to be
384 explained.
385
386 In contrast to the other two aromatic systems investigated, the photo-oxidation of 4-
387 methylcatechol (Table 1) did not result in the formation of nitrophenols in the aerosol phase
388 during initial SOA growth. In this experiment, 591 ppbv of 4-methyl catechol and 120 ppbv
389 of NO were added into the chamber, resulting in the formation of 154 μg m^{-3} of SOA mass,
390 with an SOA yield of 9.8 % (corrected for wall loss and chamber dilution). Only one
391 nitrophenol compound (MW 168 g mol^{-1}, 4-methyl-5-nitrocatechol) was observed in the
392 PILS SOA samples. The fragmentation patterns and structural assignment of this species is
393 discussed in the SI, but based on known gas-phase mechanisms and the characteristic mass
394 spectral fragmentation patterns, the most likely structure is 4-methyl-5-nitrocatechol.
395 Interestingly, 4-methyl-5-nitrocatechol was not observed in the aerosol phase until the
396 chamber covers were closed, approximately 2.5 hours after irradiation was initiated (SI

Figure S9). The observation of this species in the aerosol phase after irradiation had stopped, suggests photolytic dissociation is preventing this compound from accumulating in the gas-phase and partitioning into the aerosol phase. This also indicates that there is a dark formation source of 4-methyl-5-nitrocatechol which is most likely initiated through the rapid reaction of 4-methylcatechol with NO_3 ($13.4 \pm 5.0 \times 10^{-11}$ cm^3 $molecule^{-1}$ s^{-1})[78] followed by the addition of NO_2 to the aromatic ring.

The location of aromatic substitutions can affect the rate of reaction[79], photolytic dissociation[79, 80] (including HONO formation[63]) and the strength of hydrogen bonds owing to the change in resonance stability of the aromatic ring (should these species undergo gas-phase clustering)[75-77]. It is therefore likely that the location of aromatic substitutions in 4-methyl-5-nitrocatechol makes this compound more susceptible to a loss process such as photolysis than 3-methyl-4-nitrocatechol (observed from the photo-oxidation of toluene), accounting for the differences in the timing of partitioning observed; highlighting the importance of studying SOA formation at molecular level.

Atmospheric Relevance

In chamber experiments, the $RO_2 + RO_2$ reaction pathway favoured in relatively "low NO environments" is thought to be key to new particle formation and SOA growth in the photo-oxidation of aromatic VOC systems[48]. Here we observed that both a low NO environment and sufficient NO_2 concentration is required for the formation of ON compounds, which in the photo-oxidation of methyl chavicol represented 8 of the 13 particulate phase compounds observed during initial aerosol growth. The ON compounds at their maximum concentration represented 4.39 % of SOA mass in $MC_{[high]}$, 1.05 % in Tol_{mod} and 0.18 % in Tol_{low}, based on the average SOA mass formed during the same PILS sampling time period. In chamber

422 experiments, where NO_x is not replenished, the NO_2 concentration decreases below the
423 detection limit of the instrument (~ 0.6 ppbv), which is likely to reduce the formation rate of
424 the ON species. However, in the atmosphere NO_2 continuously forms within the VOC-NO_x-
425 O_3 cycle, which is likely to result in the continuous formation of these compounds in the
426 ambient atmosphere. For the toluene (no kinetic data exists for methyl chavicol) in polluted
427 environments, hydrogen atom abstraction and addition of NO_2 to the aromatic ring (2.5-3.6 ×
428 10^{-11} cm^3 $molecule^{-1}$ s^{-1})[81] is a minor, but still important, channel in competition with the
429 addition of O_2 (1.8-20 × 10^{-16} cm^3 $molecule^{-1}$ s^{-1})[82]. Close to emission sources, NO_2 will be
430 rapidly formed *via* the conversion of NO, leading to relatively high NO_2 concentrations,
431 increasing the potential to form these species[81, 82]. Peroxyacetyl nitrates (PANs) may also
432 contribute to the formation of these ON species, providing a source of NO_2 upon thermal
433 decomposition[83]. Recent literature has suggested that only pptv concentrations of ELVOCs
434 would be required to drive new particle formation and subsequent growth[26].
435
436 The chemistry simulated in these experiments will be representative of VOC emissions
437 near a pollution source (*i.e.* high NO concentrations) and their chemical transformations as
438 they travel downwind into cleaner environments (*i.e.* conversion of NO to NO_2, followed by
439 the photolysis of NO_2 to form O_3). The initial VOC:NO_x ratio in experiment $MC_{[high]}$ is
440 representative of an agro-industrialised oil palm plantation in northern Borneo (see Pereira et
441 al. (2014)[56] for further information). In the case of the toluene photo-oxidation experiments,
442 the respectively defined "low" and "moderate" NO_x experiments (VOC:NO_x 5:1 and 13:1;
443 Table 1) were performed under NO_x-limited ozone formation conditions (as often
444 experienced in southern Europe[45] and suburban China[84]). The initial VOC:NO_x ratios in both
445 the toluene and catechol (VOC:NOx = 5:1) experiments were selected using detailed

446 chemical chamber simulations to construct ozone isopleth plots (see Bloss et al. (2005)[45] for
447 further information) to give maximum ozone formation[85].
448
449 The involvement of the ON species in new particle formation and SOA growth was not
450 directly measured. However, the observation of various nitrophenols of differing volatilities
451 in the condensed phase during initial aerosol growth in the photo-oxidation of methyl
452 chavicol and toluene, suggests these compounds may be participating new particle formation
453 and/or SOA growth. Further study, such as measurements with an atmospheric pressure
454 ionisation mass spectrometer and quantum calculations of binding energies, is warranted to
455 investigate this. Using the techniques described, a greater insight and knowledge of the
456 dynamic processes affecting SOA formation and evolution on a molecular level can be
457 obtained. To our knowledge, this is the first experimental evidence of variable temporal
458 profiles of speciated SOA compounds as a function of photochemical ageing. As shown in
459 this work, the partitioning, formation and loss of individual compounds in the particle phase
460 can vary considerably with only slight changes in the chemical composition and structure.
461 Understanding why different compounds display different rates of formation and loss is
462 critical to understanding SOA formation and evolution in the ambient atmosphere.
463
464 **Acknowledgements**
465 The assistance of scientists at EUPHORE and the York Centre of Excellence in Mass
466 Spectrometry is gratefully acknowledged. The authors would also like to thank Iustinian
467 Bejan, Paco Alacreu and the participants of the TOXIC project. This work was supported by
468 Eurochamp-2 (TA Projects E2-2009-06-24-0001, E2-2011-04-19-0059) and Fundacion
469 CEAM. ARR acknowledgements the support of the National Centre for Atmospheric
470 Science. The York Centre of Excellence in Mass Spectrometry was created thanks to a major

capital investment through Science City York, supported by Yorkshire Forward with funds from the Northern Way Initiative. Fundación CEAM is partly supported by Generalitat Valenciana and the DESESTRES- Prometeo II project. EUPHORE instrumentation is partly funded by MINECO, through INNPLANTA Project: PCT-440000-2010-003 and the projects FEDER CEAM10-3E-1301 and CEAM10-3E-1302. KEP acknowledges support of a NERC PhD studentship (NE106026057).

Supporting Information

SI Tables S1 and S2 show the proposed mechanistic generations of the structurally identified compounds displaying TP1 or TP3 evolutions. Figure S1 displays the temporal profiles of the VOC precursors, NO, NO_2, O_3 and SOA mass formed, and Figure S2 displays the observed first generation gas-phase oxidation products formed in the experiments discussed. Figure S3 displays the predicted and measured condensed phase temporal profile of (4-methoxyphenyl)acetic acid. Figures S4 to S9 display the relationship of ON temporal profiles with the NO_2/NO ratio in Tol_{mod} and Tol_{low} and contour plots of particle diameter *vs.* particle mass and particle number for experiments Tol_{mod}, Tol_{low} and 4MCat. Tables S3 to S6 and Figures S10 to S13, show the mass spectral fragment ions, proposed fragmentation and the suggested ON compound structures. Finally, the PILS collection efficiency, volatility calculations, particle wall loss corrections, quantification of the observed compounds and the supporting calculations for the predicted 2-methyl-4-nitrophenol aerosol phase concentrations are discussed. This information is available free of charge via the Internet at http://pubs.acs.org/.

References

493 1. Kanakidou, M.; Seinfeld, J. H.; Pandis, S. N.; Barnes, I.; Dentener, F. J.; Facchini, M.
494 C.; Van Dingenen, R.; Ervens, B.; Nenes, A.; Nielsen, C. J.; Swietlicki, E.; Putaud, J. P.;
495 Balkanski, Y.; Fuzzi, S.; Horth, J.; Moortgat, G. K.; Winterhalter, R.; Myhre, C. E. L.;
496 Tsigaridis, K.; Vignati, E.; Stephanou, E. G.; Wilson, J., Organic aerosol and global climate
497 modelling: A review. *Atmos. Chem. Phys.* **2005,** *5*, (4), 1053.

498 2. Zhao, Y.; Kreisberg, N. M.; Worton, D. R.; Isaacman, G.; Weber, R. J.; Liu, S.; Day,
499 D. A.; Russell, L. M.; Markovic, M. Z.; VandenBoer, T. C.; Murphy, J. G.; Hering, S. V.;
500 Goldstein, A. H., Insights into secondary organic aerosol formation mechanisms from
501 measured gas/particle partitioning of specific organic tracer compounds. *Environ. Sci.*
502 *Technol.* **2013,** *47*, (8), 3781.

503 3. Williams, B.; Goldstein, A.; Kreisberg, N.; Hering, S.; Worsnop, D.; Ulbrich, I.;
504 Docherty, K.; Jimenez, J., Major components of atmospheric organic aerosol in southern
505 california as determined by hourly measurements of source marker compounds. **2010,** *10*,
506 (23), 11577.

507 4. Kroll, J. H.; Seinfeld, J. H., Chemistry of secondary organic aerosol: Formation and
508 evolution of low-volatility organics in the atmosphere. *Atmos. Environ.* **2008,** *42*, (16), 3593.

509 5. Hallquist, M.; Wenger, J. C.; Baltensperger, U.; Rudich, Y.; Simpson, D.; Claeys, M.;
510 Dommen, J.; Donahue, N. M.; George, C.; Goldstein, A. H.; Hamilton, J. F.; Herrmann, H.;
511 Hoffmann, T.; Iinuma, Y.; Jang, M.; Jenkin, M. E.; Jimenez, J. L.; Kiendler-Scharr, A.;
512 Maenhaut, W.; McFiggans, G.; Mentel, T. F.; Monod, A.; Prévôt, A. S. H.; Seinfeld, J. H.;
513 Surratt, J. D.; Szmigielski, R.; J., W., The formation, properties and impact of secondary
514 organic aerosol: Current and emerging issues. *Atmos. Chem. Phys*. **2009,** *9*, (14), 5155.

6. Hearn, J. D.; Renbaum, L. H.; Wang, X.; Smith, G. D., Kinetics and products from reaction of cl radicals with dioctyl sebacate (dos) particles in o2: A model for radical-initiated oxidation of organic aerosols. *PCCP* **2007,** *9*, (34), 4803.

7. Claeys, M.; Wang, W.; Ion, A. C.; Kourtchev, I.; Gelencsér, A.; Maenhaut, W., Formation of secondary organic aerosols from isoprene and its gas-phase oxidation products through reaction with hydrogen peroxide. *Atmos. Environ.* **2004,** *38*, (25), 4093.

8. Perri, M. J.; Seitzinger, S.; Turpin, B. J., Secondary organic aerosol production from aqueous photooxidation of glycolaldehyde: Laboratory experiments. *Atmos. Environ.* **2009,** *43*, (8), 1487.

9. George, I.; Abbatt, J., Chemical evolution of secondary organic aerosol from oh-initiated heterogeneous oxidation. *Atmos. Chem. Phys*. **2010,** *10*, (12), 5551.

10. Barsanti, K. C.; Pankow, J. F., Thermodynamics of the formation of atmospheric organic particulate matter by accretion reactions - part 1: Aldehydes and ketones. *Atmos. Environ.* **2004,** *38*, (26), 4371.

11. Kalberer, M.; Paulsen, D.; Sax, M.; Steinbacher, M.; Dommen, J.; Prevot, A.; Fisseha, R.; Weingartner, E.; Frankevich, V.; Zenobi, R., Identification of polymers as major components of atmospheric organic aerosols. *Science* **2004,** *303*, (5664), 1659.

12. Tolocka, M. P.; Jang, M.; Ginter, J. M.; Cox, F. J.; Kamens, R. M.; Johnston, M. V., Formation of oligomers in secondary organic aerosol. *Environ. Sci. Technol.* **2004,** *38*, (5), 1428.

13. Iinuma, Y.; Böge, O.; Gnauk, T.; Herrmann, H., Aerosol-chamber study of the α -pinene/o3 reaction: Influence of particle acidity on aerosol yields and products. *Atmos. Environ.* **2004,** *38*, (5), 761.

538 14. Gao, S.; Keywood, M.; Ng, N. L.; Surratt, J.; Varutbangkul, V.; Bahreini, R.; Flagan,
539 R. C.; Seinfeld, J. H., Low-molecular-weight and oligomeric components in secondary
540 organic aerosol from the ozonolysis of cycloalkenes and α-pinene. *J. Phys. Chem. A* **2004,**
541 *108*, (46), 10147.

542 15. Gao, S.; Ng, N. L.; Keywood, M.; Varutbangkul, V.; Bahreini, R.; Nenes, A.; He, J.;
543 Yoo, K. Y.; Beauchamp, J. L.; Hodyss, R. P.; Flagan, R. C.; Seinfeld, J. H., Particle phase
544 acidity and oligomer formation in secondary organic aerosol. *Environ. Sci. Technol.* **2004,** *38*,
545 (24), 6582.

546 16. Goldstein, A. H.; Galbally, I. E., Known and unexplored organic constituents in the
547 earth's atmosphere. *Environ. Sci. Technol.* **2007,** *41*, (5), 1514.

548 17. Zhang, R.; Suh, I.; Zhao, J.; Zhang, D.; Fortner, E. C.; Tie, X.; Molina, L. T.; Molina,
549 M. J., Atmospheric new particle formation enhanced by organic acids. *Science* **2004,** *304*,
550 (5676), 1487.

551 18. Donahue, N. M.; Ortega, I. K.; Chuang, W.; Riipinen, I.; Riccobono, F.;
552 Schobesberger, S.; Dommen, J.; Baltensperger, U.; Kulmala, M.; Worsnop, D. R.;
553 Vehkamaki, H., How do organic vapors contribute to new-particle formation? *Faraday*
554 *discussions* **2013, 165, (0), 91**.

555 19. Kulmala, M.; Kontkanen, J.; Junninen, H.; Lehtipalo, K.; Manninen, H. E.; Nieminen,
556 T.; Petäjä, T.; Sipilä, M.; Schobesberger, S.; Rantala, P.; Franchin, A.; Jokinen, T.; Järvinen,
557 E.; Äijälä, M.; Kangasluoma, J.; Hakala, J.; Aalto, P. P.; Paasonen, P.; Mikkilä, J.; Vanhanen,
558 J.; Aalto, J.; Hakola, H.; Makkonen, U.; Ruuskanen, T.; Mauldin, R. L.; Duplissy, J.;
559 Vehkamäki, H.; Bäck, J.; Kortelainen, A.; Riipinen, I.; Kurtén, T.; Johnston, M. V.; Smith, J.
560 N.; Ehn, M.; Mentel, T. F.; Lehtinen, K. E. J.; Laaksonen, A.; Kerminen, V.-M.; Worsnop, D.
561 R., Direct observations of atmospheric aerosol nucleation. *Science* **2013,** *339*, (6122), 943.

562 20. Donahue, N. M.; Trump, E. R.; Pierce, J. R.; Riipinen, I., Theoretical constraints on
563 pure vapor-pressure driven condensation of organics to ultrafine particles. *Geophys. Res. Lett.*
564 **2011,** *38*, (16), L16801.

565 21. Riipinen, I.; Pierce, J. R.; Yli-Juuti, T.; Nieminen, T.; Häkkinen, S.; Ehn, M.;
566 Junninen, H.; Lehtipalo, K.; Petäjä, T.; Slowik, J.; Chang, R.; Shantz, N. C.; Abbatt, J.;
567 Leaitch, W. R.; Kerminen, V. M.; Worsnop, D. R.; Pandis, S. N.; Donahue, N. M.; Kulmala,
568 M., Organic condensation: A vital link connecting aerosol formation to cloud condensation
569 nuclei (ccn) concentrations. *Atmos. Chem. Phys.* **2011,** *11*, (8), 3865.

570 22. Pierce, J. R.; Riipinen, I.; Kulmala, M.; Ehn, M.; Petäjä, T.; Junninen, H.; Worsnop,
571 D. R.; Donahue, N. M., Quantification of the volatility of secondary organic compounds in
572 ultrafine particles during nucleation events. *Atmos. Chem. Phys*. **2011,** *11*, (17), 9019.

573 23. Ehn, M.; Thornton, J. A.; Kleist, E.; Sipila, M.; Junninen, H.; Pullinen, I.; Springer,
574 M.; Rubach, F.; Tillmann, R.; Lee, B.; Lopez-Hilfiker, F.; Andres, S.; Acir, I.-H.; Rissanen,
575 M.; Jokinen, T.; Schobesberger, S.; Kangasluoma, J.; Kontkanen, J.; Nieminen, T.; Kurten,
576 T.; Nielsen, L. B.; Jorgensen, S.; Kjaergaard, H. G.; Canagaratna, M.; Maso, M. D.; Berndt,
577 T.; Petaja, T.; Wahner, A.; Kerminen, V.-M.; Kulmala, M.; Worsnop, D. R.; Wildt, J.;
578 Mentel, T. F., A large source of low-volatility secondary organic aerosol. *Nature* **2014,** *506*,
579 (7489), 476.

580 24. Wang, L.; Khalizov, A. F.; Zheng, J.; Xu, W.; Ma, Y.; Lal, V.; Zhang, R.,
581 Atmospheric nanoparticles formed from heterogeneous reactions of organics. *Nature Geosci*
582 **2010,** *3*, (4), 238.

583 25. Kokkola, H.; Yli-Pirilä, P.; Vesterinen, M.; Korhonen, H.; Keskinen, H.;
584 Romakkaniemi, S.; Hao, L.; Kortelainen, A.; Joutsensaari, J.; Worsnop, D. R.; Virtanen, A.;

585 Lehtinen, K. E. J., The role of low volatile organics on secondary organic aerosol formation.
586 *Atmos. Chem. Phys.* **2014,** *14*, (3), 1689.

587 26. Donahue, N.; Ortega, I.; Chuang, W.; Riipinen, I.; Riccobono, F.; Schobesberger, S.;
588 Dommen, J.; Baltensperger, U.; Kulmala, M.; Worsnop, D.; Vehkamaki, H., How do organic
589 vapors contribute to new-particle formation? *Faraday Discuss.* **2013,** *165*, 91

590 27. DeCarlo, P. F.; Kimmel, J. R.; Trimborn, A.; Northway, M. J.; Jayne, J. T.; Aiken, A.
591 C.; Gonin, M.; Fuhrer, K.; Horvath, T.; Docherty, K. S., Field-deployable, high-resolution,
592 time-of-flight aerosol mass spectrometer. *Anal. Chem.* **2006,** *78*, (24), 8281.

593 28. Canagaratna, M. R.; Jayne, J. T.; Jimenez, J. L.; Allan, J. D.; Alfarra, M. R.; Zhang,
594 Q.; Onasch, T. B.; Drewnick, F.; Coe, H.; Middlebrook, A.; Delia, A.; Williams, L. R.;
595 Trimborn, A. M.; Northway, M. J.; DeCarlo, P. F.; Kolb, C. E.; Davidovits, P.; Worsnop, D.
596 R., Chemical and microphysical characterization of ambient aerosols with the aerodyne
597 aerosol mass spectrometer. *Mass Spectrom. Rev.* **2007,** *26*, (2), 185.

598 29. Jimenez, J. L.; Canagaratna, M. R.; Donahue, N. M.; Prevot, A. S. H.; Zhang, Q.;
599 Kroll, J. H.; DeCarlo, P. F.; Allan, J. D.; Coe, H.; Ng, N. L.; Aiken, A. C.; Docherty, K. S.;
600 Ulbrich, I. M.; Grieshop, A. P.; Robinson, A. L.; Duplissy, J.; Smith, J. D.; Wilson, K. R.;
601 Lanz, V. A.; Hueglin, C.; Sun, Y. L.; Tian, J.; Laaksonen, A.; Raatikainen, T.; Rautiainen, J.;
602 Vaattovaara, P.; Ehn, M.; Kulmala, M.; Tomlinson, J. M.; Collins, D. R.; Cubison, M. J.; E.;
603 Dunlea, J.; Huffman, J. A.; Onasch, T. B.; Alfarra, M. R.; Williams, P. I.; Bower, K.; Kondo,
604 Y.; Schneider, J.; Drewnick, F.; Borrmann, S.; Weimer, S.; Demerjian, K.; Salcedo, D.;
605 Cottrell, L.; Griffin, R.; Takami, A.; Miyoshi, T.; Hatakeyama, S.; Shimono, A.; Sun, J. Y.;
606 Zhang, Y. M.; Dzepina, K.; Kimmel, J. R.; Sueper, D.; Jayne, J. T.; Herndon, S. C.;
607 Trimborn, A. M.; Williams, L. R.; Wood, E. C.; Middlebrook, A. M.; Kolb, C. E.;

608 Baltensperger, U.; Worsnop, D. R., Evolution of organic aerosols in the atmosphere. *Science*
609 **2009,** *326*, (5959), 1525.

610 30. Laskin, A.; Laskin, J.; Nizkorodov, S. A., Mass spectrometric approaches for
611 chemical characterisation of atmospheric aerosols: Critical review of the most recent
612 advances. *Environ. Chem.* **2012,** *9*, (3), 163.

613 31. Zhang, Q.; Jimenez, J. L.; Canagaratna, M. R.; Allan, J. D.; Coe, H.; Ulbrich, I.;
614 Alfarra, M. R.; Takami, A.; Middlebrook, A. M.; Sun, Y. L.; Dzepina, K.; Dunlea, E.;
615 Docherty, K.; DeCarlo, P. F.; Salcedo, D.; Onasch, T.; Jayne, J. T.; Miyoshi, T.; Shimono,
616 A.; Hatakeyama, S.; Takegawa, N.; Kondo, Y.; Schneider, J.; Drewnick, F.; Borrmann, S.;
617 Weimer, S.; Demerjian, K.; Williams, P.; Bower, K.; Bahreini, R.; Cottrell, L.; Griffin, R. J.;
618 Rautiainen, J.; Sun, J. Y.; Zhang, Y. M.; Worsnop, D. R., Ubiquity and dominance of
619 oxygenated species in organic aerosols in anthropogenically-influenced northern hemisphere
620 midlatitudes. *Geophys. Res. Lett.* **2007,** *34*, (13), L13801.

621 32. Li, K.; Wang, W.; Ge, M.; Li, J.; Wang, D., Optical properties of secondary organic
622 aerosols generated by photooxidation of aromatic hydrocarbons. *Sci. Rep.* **2014,** *4*, 4922 .

623 33. Singh, H. B.; Salas, L. J.; Cantrell, B. K.; Redmond, R. M., Distribution of aromatic
624 hydrocarbons in the ambient air. *Atmos. Environ. (1967)* **1985,** *19*, (11), 1911.

625 34. Na, K.; Moon, K.-C.; Kim, Y. P., Source contribution to aromatic voc concentration
626 and ozone formation potential in the atmosphere of seoul. *Atmos. Environ.* **2005,** *39*, (30),
627 5517.

628 35. Suthawaree, J.; Tajima, Y.; Khunchornyakong, A.; Kato, S.; Sharp, A.; Kajii, Y.,
629 Identification of volatile organic compounds in suburban bangkok, thailand and their
630 potential for ozone formation. *Atmos. Res.* **2012,** *104*, 245.

631 36. Zi-feng, L.; Ji-ming, H. A. O.; Jing-chun, D.; Jun-hua, L. I., Estimate of the formation
632 potential of secondary organic aerosol in beijing summertime. *Huan Jing Ke Xue* **2009,** *30*,
633 969.

634 37. Liu, S.; Ahlm, L.; Day, D. A.; Russell, L. M.; Zhao, Y.; Gentner, D. R.; Weber, R. J.;
635 Goldstein, A. H.; Jaoui, M.; Offenberg, J. H., Secondary organic aerosol formation from
636 fossil fuel sources contribute majority of summertime organic mass at bakersfield. *J.*
637 *Geophys. Res. Atmos.* **2012,** 177, (D24).

638 38. Lü, Z.; Hao, J.; Duan, J.; Li, J., Estimate of the formation potential of secondary
639 organic aerosol in beijing summertime. *Huan jing ke xue= Huanjing kexue/[bian ji,*
640 *Zhongguo ke xue yuan huan jing ke xue wei yuan hui" Huan jing ke xue" bian ji wei yuan*
641 *hui.]* **2009,** *30*, (4), 969.

642 39. de Gouw, J. A.; Brock, C. A.; Atlas, E. L.; Bates, T. S.; Fehsenfeld, F. C.; Goldan, P.
643 D.; Holloway, J. S.; Kuster, W. C.; Lerner, B. M.; Matthew, B. M.; Middlebrook, A. M.;
644 Onasch, T. B.; Peltier, R. E.; Quinn, P. K.; Senff, C. J.; Stohl, A.; Sullivan, A. P.; Trainer,
645 M.; Warneke, C.; Weber, R. J.; Williams, E. J., Sources of particulate matter in the
646 northeastern united states in summer: 1. Direct emissions and secondary formation of organic
647 matter in urban plumes. *J. Geophys. Res. Atmos.* **2008,** 113, (D8).

648 40. Odum, J. R.; Jungkamp, T. P. W.; Griffin, R. J.; Flagan, R. C.; Seinfeld, J. H., The
649 atmospheric aerosol-forming potential of whole gasoline vapor. *Science* **1997,** *276*, (5309),
650 96.

651 41. Gentner, D. R.; Isaacman, G.; Worton, D. R.; Chan, A. W. H.; Dallmann, T. R.;
652 Davis, L.; Liu, S.; Day, D. A.; Russell, L. M.; Wilson, K. R.; Weber, R.; Guha, A.; Harley, R.
653 A.; Goldstein, A. H., Elucidating secondary organic aerosol from diesel and gasoline vehicles

654 through detailed characterization of organic carbon emissions. *Proceedings of the National*
655 *Academy of Sciences* **2012,** *109*, (45), 18318.

656 42. Odum, J. R.; Jungkamp, T. P. W.; Griffin, R. J.; Forstner, H. J. L.; Flagan, R. C.;
657 Seinfeld, J. H., Aromatics, reformulated gasoline, and atmospheric organic aerosol formation.
658 *Environ. Sci. Technol.* **1997,** *31*, (7), 1890.

659 43. Xiao, H.; Zhu, B., Modelling study of photochemical ozone creation potential of non-
660 methane hydrocarbon. *Water, Air, Soil Pollut.* **2003,** *145*, (1-4), 3.

661 44. Derwent, R.; Jenkin, M.; Passant, N.; Pilling, M., Reactivity-based strategies for
662 photochemical ozone control in europe. *Environ. Sci. Policy* **2007,** *10*, (5), 445.

663 45. Bloss, C.; Wagner, V.; Bonzanini, A.; Jenkin, M. E.; Wirtz, K.; Martin-Reviejo, M.;
664 Pilling, M. J., Evaluation of detailed aromatic mechanisms (mcmv3 and mcmv3.1) against
665 environmental chamber data. *Atmos. Chem. Phys.* **2005,** *5*, (3), 623.

666 46. Hurley, M. D.; Sokolov, O.; Wallington, T. J.; Takekawa, H.; Karasawa, M.; Klotz,
667 B.; Barnes, I.; Becker, K. H., Organic aerosol formation during the atmospheric degradation
668 of toluene. *Environ. Sci. Technol.* **2001,** *35*, (7), 1358.

669 47. Johnson, D.; Jenkin, M. E.; Wirtz, K.; Martin-Reviejo, M., Simulating the formation
670 of secondary organic aerosol from the photooxidation of toluene. *Environ. Chem.* **2004,** *1*,
671 (3), 150.

672 48. Song, C.; Na, K.; Warren, B.; Malloy, Q.; Cocker, D. R., Secondary organic aerosol
673 formation from the photooxidation of p- and o-xylene. *Environ. Sci. Technol.* **2007,** *41*, (21),
674 7403.

675 49. Ng, N.; Kroll, J.; Chan, A.; Chhabra, P.; Flagan, R.; Seinfeld, J., Secondary organic
676 aerosol formation from m-xylene, toluene, and benzene. *Atmos. Chem. Phys.* **2007,** *7*, (14),
677 3909.

678 50. Becker, K., Euphore: Final report to the european commission. *Contract EV5V-CT92-*
679 *0059, Bergische Universität Wuppertal, Germany* **1996**.

680 51. Klotz, B.; Sørensen, S.; Barnes, I.; Becker, K. H.; Etzkorn, T.; Volkamer, R.; Platt,
681 U.; Wirtz, K.; Martín-Reviejo, M., Atmospheric oxidation of toluene in a large-volume
682 outdoor photoreactor: In situ determination of ring-retaining product yields. *J. Phys. Chem.*
683 *A.* **1998,** *102*, (50), 10289.

684 52. Volkamer, R.; Platt, U.; Wirtz, K.; Barnes, I.; Sidebottom, H. *The european*
685 *photoreactor (euphore), 3rd annual report 2000*; Bergische Universität Wuppertal
686 Wuppertal, Germany: 2001.

687 53. Muñoz, A.; Vera, T.; Sidebottom, H.; Mellouki, A.; Borrás, E.; Ródenas, M.;
688 Clemente, E.; Vázquez, M., Studies on the atmospheric degradation of chlorpyrifos-methyl.
689 *Environ. Sci. Technol.* **2011,** *45*, (5), 1880.

690 54. Carter, W.; Atkinson, R.; Winer, A.; Pitts, J., Evidence for chamber-dependent radical
691 sources: Impact on kinetic computer models for air pollution. *Int. J. Chem. Kinet.* **1981,** *13*,
692 (8), 735.

693 55. Akimoto, H.; Takagi, H.; Sakamaki, F., Photoenhancement of the nitrous acid
694 formation in the surface reaction of nitrogen dioxide and water vapor: Extra radical source in
695 smog chamber experiments. *Int. J. Chem. Kinet.* **1987,** *19*, (6), 539.

696 56. Pereira, K. L.; Hamilton, J. F.; Rickard, A. R.; Bloss, W. J.; Alam, M. S.; Camredon,
697 M.; Muñoz, A.; Vázquez, M.; Borrás, E.; Ródenas, M., Secondary organic aerosol formation

698 and composition from the photo-oxidation of methyl chavicol (estragole). *Atmos. Chem.*
699 *Phys.* **2014,** *14*, (11), 5349.

700 57. Donahue, N.; Robinson, A.; Stanier, C.; Pandis, S., Coupled partitioning, dilution, and
701 chemical aging of semivolatile organics. *Environ. Sci. Technol.* **2006,** *40*, (8), 2635.

702 58. Stanier, C. O.; Donahue, N.; Pandis, S. N., Parameterization of secondary organic
703 aerosol mass fractions from smog chamber data. *Atmos. Environ.* **2008,** *42*, (10), 2276.

704 59. Pankow, J. F., An absorption model of the gas/aerosol partitioning involved in the
705 formation of secondary organic aerosol. *Atmos. Environ.* **1994,** *28*, (2), 189.

706 60. Pankow, J. F., An absorption model of gas/particle partitioning of organic compounds
707 in the atmosphere. *Atmos. Environ.* **1994,** *28*, (2), 185.

708 61. Jenkin, M. E.; Saunders, S. M.; Pilling, M. J., The tropospheric degradation of volatile
709 organic compounds: A protocol for mechanism development. *Atmos. Environ.* **1997,** *31*, (1),
710 81.

711 62. Bröske, R.; Kleffmann, J.; Wiesen, P., Heterogeneous conversion of no2 on secondary
712 organic aerosol surfaces: A possible source of nitrous acid (hono) in the atmosphere? *Atmos.*
713 *Chem. Phys.* **2003,** *3*, (3), 469.

714 63. Bejan, I.; Abd El Aal, Y.; Barnes, I.; Benter, T.; Bohn, B.; Wiesen, P.; Kleffmann, J.,
715 The photolysis of ortho-nitrophenols: A new gas phase source of hono. *PCCP* **2006,** *8*, (17),
716 2028.

717 64. Kleffmann, J., Daytime sources of nitrous acid (hono) in the atmospheric boundary
718 layer. *J. Chem. Phys. Phys. Chem.* **2007,** *8*, (8), 1137.

719 65. Forstner, H. J. L.; Flagan, R. C.; Seinfeld, J. H., Secondary organic aerosol from the
720 photooxidation of aromatic hydrocarbons: Molecular composition. *Environ. Sci. Technol.*
721 **1997,** *31*, (5), 1345.

722 66. Jang, M.; Kamens, R. M., Characterization of secondary aerosol from the
723 photooxidation of toluene in the presence of nox and 1-propene. *Environ. Sci. Technol.* **2001,**
724 *35*, (18), 3626.

725 67. Hamilton, J. F.; Webb, P. J.; Lewis, A. C.; Reviejo, M. M., Quantifying small
726 molecules in secondary organic aerosol formed during the photo-oxidation of toluene with
727 hydroxyl radicals. *Atmos. Environ.* **2005,** *39*, (38), 7263.

728 68. Sato, K.; Hatakeyama, S.; Imamura, T., Secondary organic aerosol formation during
729 the photooxidation of toluene: Nox dependence of chemical composition. *J. Phys. Chem. A.*
730 **2007,** *111*, (39), 9796.

731 69. Zhong, M.; Jang, M.; Oliferenko, A.; Pillai, G. G.; Katritzky, A. R., The soa
732 formation model combined with semiempirical quantum chemistry for predicting uv-vis
733 absorption of secondary organic aerosols. *PCCP* **2012,** *14*, (25), 9058.

734 70. Sato, K.; Takami, A.; Kato, Y.; Seta, T.; Fujitani, Y.; Hikida, T.; Shimono, A.;
735 Imamura, T., Ams and lc/ms analyses of soa from the photooxidation of benzene and 1, 3, 5-
736 trimethylbenzene in the presence of no x: Effects of chemical structure on soa aging. *Atmos.*
737 *Chem. Phys.* **2012,** *12*, (10), 4667.

738 71. Cabral do Couto, P.; Guedes, R. C.; Costa Cabral, B. J.; Martinho Simões, J. A.,
739 Phenol o–h bond dissociation energy in water clusters. *Int. J. Quantum Chem* **2002,** *86*, (3),
740 297.

741 72. Parthasarathi, R.; Subramanian, V.; Sathyamurthy, N., Hydrogen bonding in phenol,
742 water, and phenol−water clusters. *J. Phys. Chem. A.* **2005,** *109*, (5), 843.

743 73. Tsui, H. H. Y.; van Mourik, T., Ab initio calculations on phenol–water. *Chem. Phys.*
744 *Lett.* **2001,** *350*, (5–6), 565.

745 74. Benoit, D. M.; Clary, D. C., Quantum simulation of phenol−water clusters. *J. Phys.*
746 *Chem. A.* **2000,** *104*, (23), 5590.

747 75. An, X.; Jing, B.; Li, Q., Regulating function of alkali metal on the strength of oh···o
748 hydrogen bond in phenol–water complex: Weak to strong and strong to weak. *Comp.Theor.*
749 *Chem.* **2011,** *966*, (1–3), 278.

750 76. Chen, P. C.; Chen, S. C., Theoretical study of the internal rotational barriers in
751 nitrobenzene, 2-nitrotoluene, 2-nitrophenol, and 2-nitroaniline. *Int. J. Quantum Chem* **2001,**
752 *83*, (6), 332.

753 77. Chen, P. C.; Lo, W.; Tzeng, S. C., Molecular structures of mononitrophenols and their
754 thermal decomposition tautomers. *J. Mol. Struct.* **1998,** *428*, (1–3), 257.

755 78. Olariu, R. I.; Bejan, I.; Barnes, I.; Klotz, B.; Becker, K. H.; Wirtz, K., Rate
756 coefficients for the gas-phase reaction of no3 radicals with selected dihydroxybenzenes. *Int.*
757 *J. Chem. Kinet.* **2004,** *36*, (11), 577.

758 79. Bejan, I. G. Investigations on the gas phase atmospheric chemistry of nitrophenols
759 and catechols. Bergische University of Wupperthal, Germany, 2006.

760 80. Chen, J.; Wenger, J. C.; Venables, D. S., Near-ultraviolet absorption cross sections of
761 nitrophenols and their potential influence on tropospheric oxidation capacity. *J. Phys. Chem.*
762 *A.* **2011,** *115*, (44), 12235.

763 81. Atkinson, R.; Aschmann, S. M., Products of the gas-phase reactions of aromatic
764 hydrocarbons: Effect of no2 concentration. *Int. J. Chem. Kinet.* **1994,** *26*, (9), 929.

765 82. Atkinson, R., Atmospheric chemistry of vocs and nox. *Atmos. Environ.* **2000,** *34*, (12-
766 14), 2063.

767 83. Orlando, J. J.; Tyndall, G. S.; Calvert, J. G., Thermal decomposition pathways for
768 peroxyacetyl nitrate (pan): Implications for atmospheric methyl nitrate levels. *Atmos.*
769 *Environ. Part A. General Topics* **1992,** *26*, (17), 3111.

770 84. Zou, Y.; Deng, X. J.; Zhu, D.; Gong, D. C.; Wang, H.; Li, F.; Tan, H. B.; Deng, T.;
771 Mai, B. R.; Liu, X. T.; Wang, B. G., Characteristics of 1 year of observational data of vocs,
772 nox and o3 at a suburban site in guangzhou, china. *Atmos. Chem. Phys.* **2015,** *15*, (12), 6625.

773 85. Bloss, C.; Wagner, V.; Jenkin, M. E.; Volkamer, R.; Bloss, W. J.; Lee, J. D.; Heard,
774 D. E.; Wirtz, K.; Martin-Reviejo, M.; Rea, G.; Wenger, J. C.; Pilling, M. J., Development of
775 a detailed chemical mechanism (mcmv3.1) for the atmospheric oxidation of aromatic
776 hydrocarbons. *Atmos. Chem. Phys.* **2005,** *5*, (3), 641.

Table 1 - Initial mixing ratios of the oxidants and VOC precursors investigated, including chamber humidity and chamber temperature for the experiments performed during the TOXIC and ATMECH project.

Project	Date	Exp.	Exp. Description	Initial mixing ratio[a]			Oxidant initial mixing ratio[a]			VOC:NO_x	Experimental range[b]	
				Toluene [ppbv]	Methyl chavicol [ppbv]	4-Methyl Catechol [ppbv]	NO [ppbv]	NO_2 [ppbv]	O_3 [ppbv]		RH [%]	Temperature [K]
TOXIC	20.07.09	Tol_{low}	Low NO_x	535	-	-	41	< LOD	< LOD	~13:1	0.2 – 2.9	297 - 308
	21.07.09	Tol_{mod}	Moderate NO_x	560	-	-	105	< LOD	< LOD	~5:1	1.1 – 2.1	297 - 309
	28.07.09	4-MCat		-	-	591	120	2	< LOD	~5:1	0.2 – 8.8	298 - 305
ATMECH	15.05.12	$MC_{[high]}$		-	460	-	92	3	5	~5:1	2.1 -10.7	297 - 306

[a] = On the opening of the chamber covers. [b] = From the opening to the closing of the chamber covers.

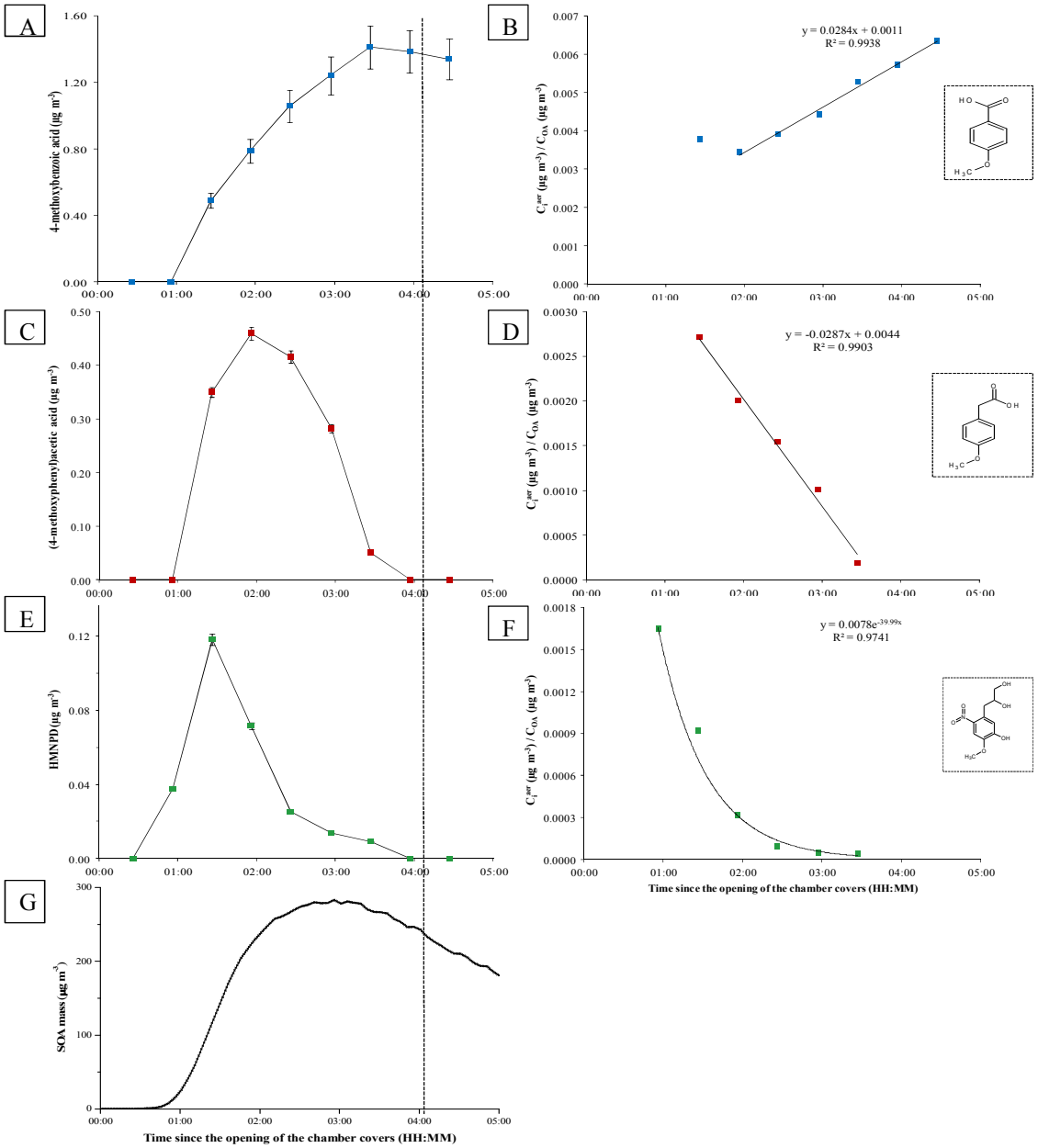

Figure 1 - Types of characteristic particulate phase temporal profile shapes observed in $MC_{[high]}$ (*left*) and their measured mass fraction ($y_i = C_{i,aer}/C_{OA}$) over time (*right*). A = TP1, 4-methoxybenzoic acid. B = 4-methoxybenzoic acid (µg m^{-3})/ average SOA mass (µg m^{-3}). C = TP2, (4-methoxyphenyl)acetic acid. D = (4-methoxyphenyl)acetic acid (µg m^{-3})/ average SOA mass (µg m^{-3}). E = TP3, HMNPD (3-(5-hydroxy-4-methoxy-2-nitrophenyl)propane-1,2-diol). F = HMNPD (3-(5-hydroxy-4-methoxy-2-nitrophenyl)propane-1,2-diol) (µg m^{-3})/ average SOA mass (µg m^{-3}). G = SOA mass. Compound structures are shown in the boxes.

Temporal profiles are plotted using the average PILS sampling time. Error bars display the average %RSD of the calibration graph used to determine the compound concentrations (see SI for further information). Dashed vertical line = closing of the chamber covers.

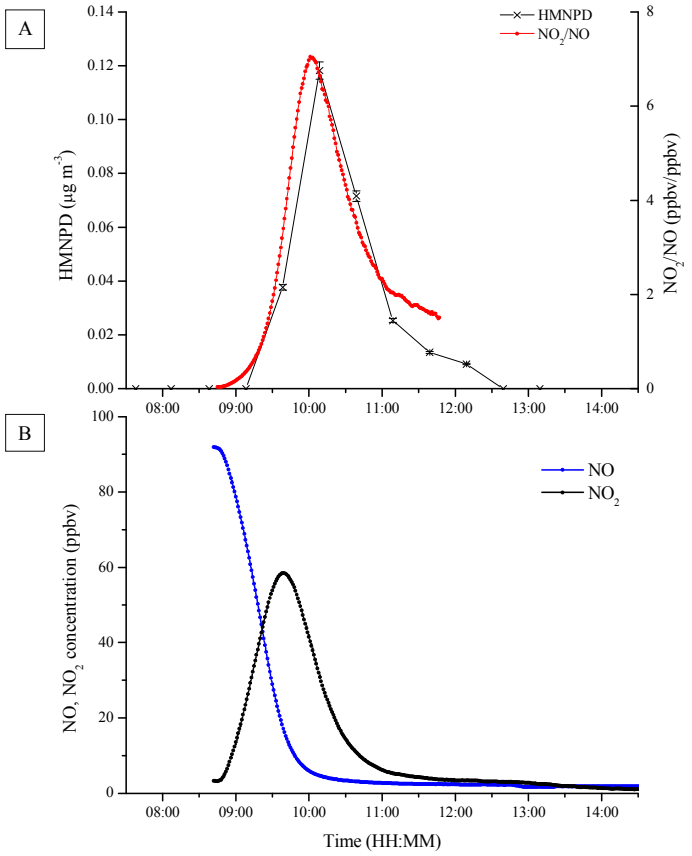

Figure 2 – Temporal profile of the NO_2/NO concentration ratio (ppbv/ppbv) and the particulate phase temporal profile of HMNPD (3-(5-hydroxy-4-methoxy-2-nitrophenyl)propane-1,2-diol, SI compound 1, Table S2) in $MC_{[high]}$. (A) Black = particulate phase temporal evolution of 3-(5-hydroxy-4-methoxy-2-nitrophenyl)propane-1,2-diol. Red = temporal profile of the NO_2/NO ratio (ppbv/ppbv). (B) Blue = NO (ppbv). Black = NO_2 (ppbv).

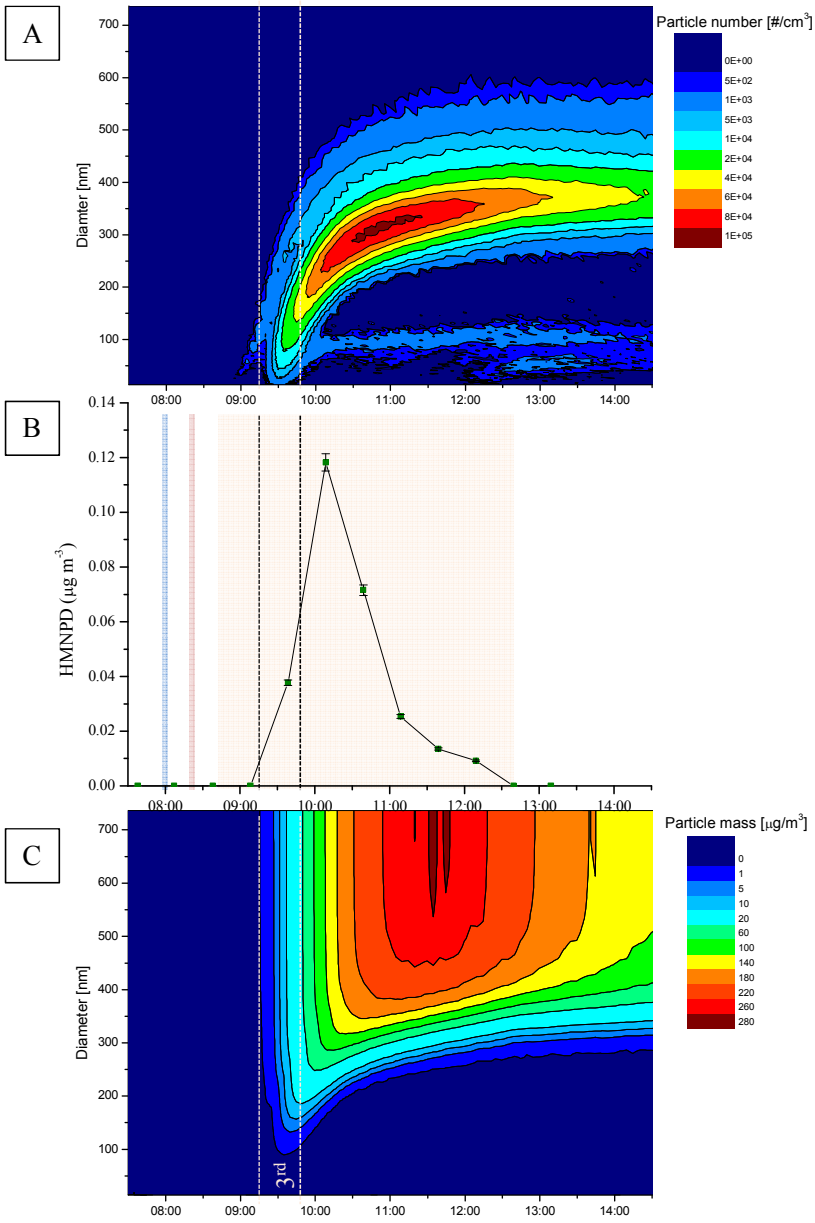

Figure 3 - Particle diameter *vs.* time with a coloured contour plot displaying increasing particle number (A) and particle mass (C), compared with the particulate phase temporal profile of HMNPD (3-(5-hydroxy-4-methoxy-2-nitrophenyl)propane-1,2-diol) (B) (SI compound 1, Table S1) during $MC_{[high]}$. Shaded areas in (B); Blue = NO addition. Red = methyl chavicol addition. Orange = opening to the closing of the chamber covers. Dashed lines display the first PILS sampling period where SOA was first observed (3rd sample from the opening of the chamber covers).

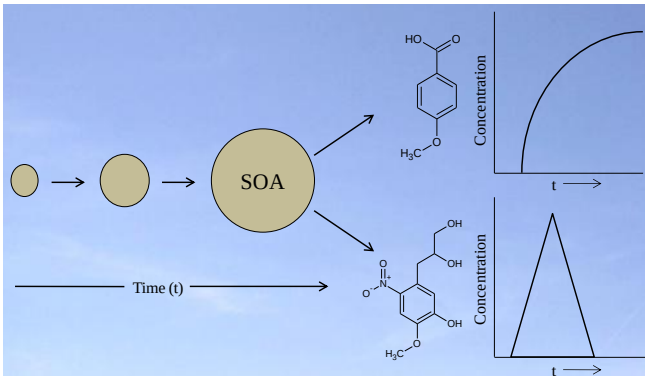
SOA
Time (t)
HO
O
H3C
O
Concentration
t
OH
OH
OH
O
N+
O
H3C
O
Concentration
t